JOURNAL OF GEOPHYSICAL RESEARCH, VOL. 114, B11103, doi:10.1029/2008JB006235, 2009

Thermal conductivity of hydrate-bearing sediments

Douglas D. Cortes,[1] Ana I. Martin,[2] Tae Sup Yun,[3] Franco M. Francisca,[4] J. Carlos Santamarina,[1] and Carolyn Ruppel[5]

Received 1 December 2008; revised 8 June 2009; accepted 23 July 2009; published 18 November 2009.

[1] A thorough understanding of the thermal conductivity of hydrate-bearing sediments is necessary for evaluating phase transformation processes that would accompany energy production from gas hydrate deposits and for estimating regional heat flow based on the observed depth to the base of the gas hydrate stability zone. The coexistence of multiple phases (gas hydrate, liquid and gas pore fill, and solid sediment grains) and their complex spatial arrangement hinder the a priori prediction of the thermal conductivity of hydrate-bearing sediments. Previous studies have been unable to capture the full parameter space covered by variations in grain size, specific surface, degree of saturation, nature of pore filling material, and effective stress for hydrate-bearing samples. Here we report on systematic measurements of the thermal conductivity of air dry, water- and tetrohydrofuran (THF)-saturated, and THF hydrate–saturated sand and clay samples at vertical effective stress of 0.05 to 1 MPa (corresponding to depths as great as 100 m below seafloor). Results reveal that the bulk thermal conductivity of the samples in every case reflects a complex interplay among particle size, effective stress, porosity, and fluid-versus-hydrate filled pore spaces. The thermal conductivity of THF hydrate–bearing soils increases upon hydrate formation although the thermal conductivities of THF solution and THF hydrate are almost the same. Several mechanisms can contribute to this effect including cryogenic suction during hydrate crystal growth and the ensuing porosity reduction in the surrounding sediment, increased mean effective stress due to hydrate formation under zero lateral strain conditions, and decreased interface thermal impedance as grain-liquid interfaces are transformed into grain-hydrate interfaces.

Citation: Cortes, D. D., A. I. Martin, T. S. Yun, F. M. Francisca, J. C. Santamarina, and C. Ruppel (2009), Thermal conductivity of hydrate-bearing sediments, *J. Geophys. Res.*, *114*, B11103, doi:10.1029/2008JB006235.

1. Introduction

[2] The formation and dissociation of gas hydrate involve a significant change in energy (e.g., 338.7 J g^{-1} at 273 K in the case of structure I methane hydrate) [*Handa*, 1986]. Phase transformation, including dissociation for the purposes of energy production from methane hydrates, may therefore be limited by thermal transport in the bulk medium, which includes not only hydrate, but also mineral grains and non-hydrate pore fill. The thermal properties of hydrate-bearing sediments are also critical for estimating regional heat flow from the observed depth of the bottom simulating reflection (BSR) that marks the base of the gas hydrate stability zone in some marine settings [e.g., *Yamano et al.*, 1982; *Grevemeyer and Villinger*, 2001] and for analysis of thermal gradients measured within hydrate-bearing sediments [e.g., *Tzirita*, 1992; *Ruppel*, 2000]. Adoption of incorrect thermal conductivity values for hydrate-bearing sediments interspersed with hydrate-free sediments can result in errors in estimated heat flow.

[3] Thermal conductivity is the key property that controls the transfer of thermal energy, yet data on the thermal conductivity of hydrate-bearing sediments remain limited. Several studies have focused on determining the thermal conductivity of gas hydrate in the absence of sediments [e.g., *Cook and Leaist*, 1983; *deMartin*, 2001; *Huang and Fan*, 2005; *Ross and Andersson*, 1982; *Waite et al.*, 2002, 2005] and often at pressure temperature conditions that do not occur in nature. Some of these studies had significant experimental difficulties such as the formation of water ice. Because these studies focus only on the gas hydrate phase, the results sometimes have limited applicability to heat transfer processes in multicomponent natural systems consisting of mineral grains, a hydrate phase, and other pore filling material (gas or liquid).

[4] Researchers have also measured the in situ thermal conductivity of hydrate-bearing sediments in permafrost [*Henninges et al.*, 2005] and marine [e.g., *Tréhu*, 2006] settings. While such analyses advance understanding of bulk in situ thermal properties, the data are of limited utility for

[1]School of Civil and Environmental Engineering, Georgia Institute of Technology, Atlanta, Georgia, USA.
[2]Atlanta, Georgia, USA.
[3]School of Civil and Environmental Engineering, Yonsei University, Seoul, South Korea.
[4]Facultad de Ingenieria, Universidad Nacional de Cordoba, Cordoba, Argentina.
[5]U.S. Geological Survey, Woods Hole, Massachusetts, USA.

0148-0227/09/2008JB006235$09.00

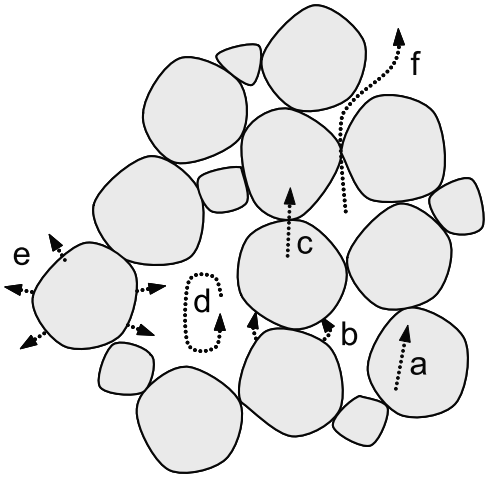

Figure 1. Primary particle-level heat transport processes in granular materials according to the processes identified by *Yun and Santamarina* [2007]: (a) Conduction along the mineral, (b) particle-fluid-particle conduction across the fluid near contacts, (c) particle-to-particle conduction across contacts, (d) fluid convection within large pores, (e) particle-fluid conduction, and (f) conduction along the pore fluid within the pore space (hydrostatic and advecting pore fluid).

understanding the impact of various parameters or processes on the thermal conductivity of hydrate-bearing sediments. The primary challenge is the inability to accurately assess in situ hydrate saturations and to constrain the microscale arrangement of mineral grains, hydrate, and other pore filling components. Without such detailed information, evaluating the significance of the in situ thermal conductivity data for other hydrate-bearing sediment regimes is impossible.

[5] A major challenge in the study of hydrate-bearing sediments has been the difficulty of forming methane hydrate in the laboratory on reasonable time scales. In marine settings, most gas hydrate probably forms from aqueous phase, not gaseous, methane [*Buffett and Zatsepina*, 2000]. This gas-limited process, whether dependent on diffusive or advective transport of the gas, is too slow for routine use in the laboratory, although some recent studies have reported progress in overcoming this obstacle [e.g., *Spangenberg et al.*, 2005; *Waite et al.*, 2008b]. Methane hydrate can be formed rapidly in the laboratory by percolating methane gas through soils [e.g., *Helgerud*, 2001; *Waite et al.*, 2004] or using the ice seed method [*Stern et al.*, 1996, 1998], and published laboratory studies on the thermal conductivity of methane hydrate-bearing sediments rely on one of these techniques [e.g., *Waite et al.*, 2002; *Tzirita*, 1992]. Unfortunately, both techniques bias the pore scale distribution of hydrates within the soil matrix, alter the interaction among hydrate, pore fluid and sediment grains, and affect many physical properties, including seismic velocities, mechanical strength, and thermal conductivity [*Lee*, 2007; *Lee et al.*, 2007; *Santamarina and Ruppel*, 2008; *Yun et al.*, 2007].

[6] Several previous studies have examined the thermal conductivity of synthetic hydrate-bearing sediments over a limited parameter space. Due to a variety of experimental and logistical constraints, such studies have been conducted with a single soil (i.e., single grain size/specific surface), at a single confining stress, with a single pore filling phase in addition to hydrate (gas or fluid), and/or without comparison to saturated and dry soil samples lacking hydrate [e.g., *Stoll and Bryan*, 1979; *Waite et al.*, 2002; *Huang and Fan*, 2005; *Henninges*, 2007]. *Tzirita* [1992] completed an early laboratory study on hydrate-bearing sands and clays and concluded that porosity was a critical factor in controlling the thermal conductivity. *deMartin* [2001] conducted experiments on hydrate-bearing sand and pure methane hydrate. His results showed that methane hydrate played an important role in increasing grain-to-grain heat transfer and thus thermal conductivity in hydrate-bearing sands and that increased effective stress led to increased grain-to-grain conduction.

[7] This study documents a systematic approach to the experimental determination of the thermal conductivity of hydrate-bearing samples. We consider the impact of hydrate formation, grain size and effective stress on bulk thermal conductivity. The results highlight the considerable complexity of heat transfer mechanisms in dry, saturated, and hydrate-bearing clay and sand samples and can potentially contribute to an understanding of the results obtained by earlier workers [e.g., *deMartin*, 2001] in more limited laboratory experiments.

2. Background: Heat Transfer in Granular Media

[8] Heat transfer takes place through convection, radiation, and conduction. In granular media, the relative contribution of free convective heat transport gains relevance in coarse grained soils characterized by a mean grain size greater than 6 mm [*Thalmann*, 1950]. On the other hand, radiative heat transport occurs through photon emissions and electromagnetic wave propagation and is only significant at temperatures above ~500°C [*Guéguen and Palciauskas*, 1994]. Therefore, heat transport in fine sands and clays at low temperatures is conductive, and the thermal conductivity is the key parameter governing heat transfer.

[9] The thermal conductivities of grains and fluids vary across several orders of magnitude: mineral grains (order of 10 W m^{-1} K^{-1}), water (order of 1 W m^{-1} K^{-1}), and air (order of 0.01 W m^{-1} K^{-1}). Such a contrast in thermal conductivities leads to preferential particle-level heat transport processes in granular materials: conduction along the mineral, particle-to-particle conduction across contacts, particle-fluid-particle conduction across the fluid near contacts, and conduction along the pore fluid within the pore space (Figure 1) [*Yun and Santamarina*, 2007]. The main factors that determine the bulk thermal conductivity of soils follow from the particle level transport process and include the volumetric fractions and properties of the constituents and the spatial arrangement and degree of connectivity of the grains.

2.1. Mineralogy

[10] The thermal conductivity of quartz is higher than other common soil forming minerals. Thus, the thermal conductivity of sediments is proportional to the volumetric fraction of quartz [*Gangadhara Rao and Singh*, 1999; *Tarnawski et al.*, 2002].

2.2. Particle Size

[11] Interparticle conductive heat transfer is proportional to the particle radius and inversely proportional to the

Table 1. Index Properties of Tested Soils as Reported by *Guimaraes* [2001], *Klein* [1999], and *Santamarina and Cho* [2001][a]

Soil	d_{50}[b] (μm)	Specific Gravity	Specific Surface ($m^2\ g^{-1}$)	n_{max}/n_{min}[c]	Sphericity	Roundness
Sand (F110)	120	2.65	0.019	0.46/0.35	0.7	0.7
Clay (SA1 kaolinite)	1.1	2.6	36–37[d]	—	0.7	0.1

[a]SEM photos of the soils and additional information can be found in *Yun et al.* [2007] and *Palomino and Santamarina* [2005].
[b]Here d_{50} is mean grain size.
[c]Maximum and minimum dry porosity.
[d]Measured by the wet (methylene blue) method.

intercontact distance [*Batchelor and O'Brien*, 1977]. Thus larger particles lead to higher thermal conductivity [*Aduda*, 1996; *Gangadhara Rao and Singh*, 1999; *Tarnawski et al.*, 2002].

2.3. Packing Density and Coordination Number

[12] Interparticle contacts play an important role in heat transfer processes. The higher the packing density and coordination number, the higher the thermal conductivity of the sediment [*Tarnawski et al.*, 2002].

2.4. Water Content

[13] Water acts as a relatively high conductivity bridge between particles. Therefore, the thermal conductivity of partially saturated soils increases with the degree of saturation [*Andersland and Ladanyi*, 2004; *Farouki*, 1985; *Lu et al.*, 2007; *Singh and Devid*, 2000]. This observation applies to hydrate-bearing sediments during dissociation and gas production, when mineral, hydrate, gas, and liquid coexist.

2.5. Effective Stress

[14] The increase in packing density, coordination number, and contact quality with increasing effective stress leads to higher thermal conductivity. Load-bearing granular chains within the soil skeleton greatly facilitate heat transfer [*Batchelor and O'Brien*, 1977; *Lambert and Fletcher*, 1997; *Sridhar and Yovanovich*, 1996; *Vargas and McCarthy*, 2001].

[15] Numerous theoretical, empirical, and semiempirical models have been developed to predict the effective thermal conductivity of composite natural materials, yet only a few of them account for the interconnectivity of the high thermal conductivity mineral phase and the quality of thermal contacts [e.g., *Droval et al.*, 2006; *Yagi and Kunii*, 1957]. In fact, thermal conductivity in granular media is often overpredicted because the resistance at contacts is not properly accounted for [*Chung*, 2001].

3. Laboratory Methods

[16] We measure the thermal conductivity of hydrate-bearing sediments having different mineral grains and subject to different vertical effective stresses. The selected soils (sand and kaolinite) cover a wide range of grain sizes (d_{50} from 1 μm to 120 μm, where d_{50} refers to the diameter for which 50% of the grains have larger size) and specific surface (0.02 $m^2\ g^{-1}$ to 36 $m^2\ g^{-1}$). Table 1 provides details about the soils used for testing, with additional information given by *Yun et al.* [2007] and *Lee et al.* [2007].

3.1. Hydrate Former

[17] We use tetrahydrofuran (THF) as the hydrate former. THF (C_4H_8O) is a clear, colorless, low-viscosity fluid that has an ether-like odor, high volatility, low freezing point (~208 K), and complete miscibility with water. The THF molecule does differ from the methane molecule; in contrast to methane, THF is a structure II, not structure I, hydrate former. Yet the thermal conductivity of methane hydrate [*Waite et al.*, 2005; *Krivchikov et al.*, 2005] and THF hydrate are known to be similar (Table 2), and the behavior of THF as a hydrate former is well understood at both the molecular and pore scales [*Lee et al.*, 2007].

Table 2. Thermal Conductivity of Sample Components and Related Materials[a]

Thermal Conductivity ($W\ m^{-1}\ K^{-1}$)	Temperature (K)	Reference
	Air	
0.024	273	*Kaye and Laby* [2007]
	Water	
0.56	273	*Kaye and Laby* [2007]
0.67	353	*Kaye and Laby* [2007]
	Ice	
2.3	268	*Kaye and Laby* [2007]
3.9	173	*Kaye and Laby* [2007]
	THF·17H20 Liquid	
0.47	283	*BASF* [1998]
0.60	293	This study
	THF·17H20 Hydrate	
0.50	261	*Waite et al.* [2005]
0.51	273	*Huang and Fan* [2005]
0.58	261	This study
	CH_4 Hydrate	
0.51	263	*Waite et al.* [2005]
0.575	273	*Huang and Fan* [2005]
	Dry Sand	
1.1	—	*Andersland and Ladanyi* [2004]
0.28 to 0.48	293	This study
	Water-Saturated Sand[b]	
1.2 to 3.0	—	*Andersland and Ladanyi* [2004]
4.2	293	This study
	Sand Saturated With THF·17H20 Liquid	
3.5 to 4.2	293	This study
	Sand With 100% THF·17H20 Hydrate	
4.1 to 4.5	261	This study
	Dry Clay	
0.9	RT	*Andersland and Ladanyi* [2004]
0.074 to 0.21	293	This study
	Water-Saturated Clay[b]	
1.9 to 2.2	—	*Becker et al.* [1992]
2.1 to 2.8	293	This study
	Clay Saturated With THF·17H20 Liquid	
1.6 to 2.6	293	This study
	Clay With 100% THF·17H20 Hydrate	
2.8 to 3.0	261	This study
	Quartz	
6.5 to 11	298	*Kaye and Laby* [2007]

[a]When a range of values is reported for soil samples, the lowest and highest values, respectively, represent the thermal conductivities corresponding to the lowest and highest vertical effective stresses used in this study.
[b]Above freezing.

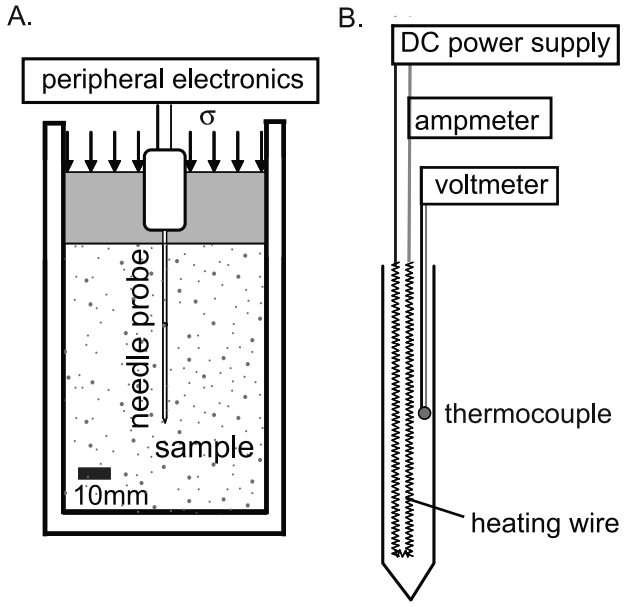

Figure 2. Laboratory devices used for these experiments: (a) zero lateral strain cell, (b) thermal needle probe and peripheral electronics.

[18] The main advantage of THF for this study is its complete miscibility in water, which means that all the THF necessary to attain a target hydrate saturation can be mixed at the beginning of the experiment. This facilitates the synthesis of specimens and allows us to properly reproduce other important geological conditions (e.g., evolution of the state of effective stress) that can play an important role in thermal conductivity. Here, we use a target fluid composition of THF $17H_2O$, which corresponds to 19% THF to 81% water by mass, to produce samples with hydrate saturation S_h of 1.0 (100% of pore space filled with hydrate). To overcome evaporation losses during mixing [*Lee et al.*, 2007; *Yun et al.*, 2007], solutions in this study are mixed at 22% THF. This also ensures that ice does not form [*Waite et al.*, 2005; *Lee et al.*, 2007].

3.2. Sample Preparation and Configuration

[19] Sediments are confined within a cylindrical stainless steel cell (inside diameter 63.5 mm, height 187.95 mm) to impose zero-lateral strain conditions (Figure 2a). We measure the vertical displacement of the top cap and compute the instantaneous porosity. Excess pore fluid can drain freely through the upper boundary; we use a supernatant oil layer seal to minimize THF evaporation throughout the testing period. During phase transformation, we maintain a constant force to attain a constant vertical effective stress condition. Pore pressure is constant at the boundaries, but may change locally within the specimen.

[20] Sand specimens are prepared by first placing the intended pore fluid into the stainless steel cell. Sand particles are then poured using a funnel held very close to the fluid surface to avoid air entrainment. The specimen is tamped regularly to attain a uniform density. When the sand reaches the desired height, excess pore fluid is removed. Filter paper is then placed on top of the specimen, followed by the loading cap and the thermal conductivity probe instrumentation. Kaolinite specimens are formed by mixing kaolin powder with the pore fluid at a mass ratio of 0.8, which is above the liquid limit (LL) of the soil, which is $LL = 0.7$ for water as pore fluid. A filter paper saturated in the pore fluid is placed along the inner perimeter of the stainless steel cell to facilitate consolidation. The kaolinite paste, held within a plastic liner, is placed inside the cell against the saturated filter paper. The liner is carefully pulled up while holding the paste in place by exerting pressure at the surface. Finally, a saturated filter paper and the loading cap are set on top of the sediment. There is no target density for the kaolinite specimen.

3.3. Thermal Conductivity Measurements

[21] The thermal conductivity of the specimens is measured with a needle probe using the technique first outlined by *Von Herzen and Maxwell* [1959]. We use an East 30 Sensors needle probe mounted on the upper cap (Figure 2a) and containing a heating wire and thermocouple (Figure 2b). A transient heat pulse is generated by imposing a DC current through the heating wire while the thermocouple monitors the temperature within the needle. The needle's length (60 mm) is much greater than its diameter (1.5 mm) so that radial conduction conditions prevail. Temperature is recorded continuously throughout the duration of the test, including during the periods of hydrate formation and dissociation. A thermal conductivity measurement consists of monitoring the input power and temperature increase every second during a 100-s-long heating interval. The typical temperature-time evolution for a given vertical effective stress is shown in Figure 3.

3.4. Experimental Sequence

[22] The test sequence for the experiments is as follows:

[23] 1. Subject the specimen to the vertical effective stress (0.05, 0.1, 0.25, 0.5 or 1 MPa, which corresponds to depths as great as ~100 m below seafloor) and allow it to consolidate at constant force until there is no further volume change. This phase endures from less than an hour in sand to over 24 h in kaolinite.

[24] 2. Determine the thermal conductivity for the consolidated unfrozen specimen under the applied vertical effective stress at room temperature during 3 separate measurements.

[25] 3. In specimens containing a mixture of THF and water, cool the specimen to a temperature between 258 and 268 K to form hydrate.

[26] 4. Determine the thermal conductivity of the hydrate-bearing sediment during four separate measurements.

[27] 5. Warm the specimen to room temperature to dissociate the hydrate. Phase transformation for THF hydrate occurs at 277 K.

[28] 6. Increase the vertical effective stress and repeat steps 1 through 5.

4. Data Reduction

[29] The general analytical solution to the line source problem in an infinite medium can be simplified for long-duration measurements to obtain the expression $\Delta T = A + B \ln(t/[s])$ [*Jones*, 1988], where ΔT denotes the change in temperature, A and B are fitting parameters, t denotes time [s] and the [s] in the denominator of the logarithm's

Table 3. Parameters Used for COMSOL®-Based Numerical Modeling

Model Element	Thermal Conductivity (W m^{-1} K^{-1})	Density (kg m^{-3})	Heat Capacity (J kg^{-1} K^{-1})
Needle probe: inner copper core	400	8700	385
Needle probe: wax layer around copper core	1.3	927	2130
Probe's cylindrical shell	44.5	7850	475

argument is included to make the total argument dimensionless. The parameter $B = q/4\pi\lambda$ is a function of the thermal conductivity λ [W m^{-1} K^{-1}] of the medium and the power q [W m^{-1}] supplied to the needle probe. Therefore the thermal conductivity can be determined from the slope of the data plotted in ΔT versus ln*(t)* space. It is often cumbersome to select the proper time range for fitting the experimental data due to the complexity of signatures recorded with real sediments and the wide range in resulting B values that can be extracted by fitting parts of the experimental data. Data fitting can be constrained using the intercept, but A is a function of the medium properties, including the thermal conductivity itself, as well as the effective heat transfer coefficient between the probe and the medium, a factor that is difficult to assess [*Jones*, 1988]. To improve data reduction, we represent the cell, the specimen, and the needle probe using finite elements, and solve the heat equation

$$\rho C \frac{dT}{dt} - \nabla \cdot (\lambda \nabla T) = Q, \tag{1}$$

in COMSOL Multiphysics® software. In (1) the parameters are density ρ [kg m^{-3}], temperature T [K], heat capacity C [J $kg^{-1}K^{-1}$], thermal conductivity λ [W m^{-1} K^{-1}], and power input Q [W m^{-3}]. The initial density of the medium is known, and the heat capacity is computed as a volumetric weighted average of the components. The needle probe is modeled with an inner copper core of 0.2 mm radius surrounded by a 0.2-mm-thick wax layer. Both the copper core and the wax layer are enclosed within a 0.25-mm-thick stainless steel cylindrical shell. The outer wall of the stainless steel cell (31.7 mm inner radius and 6.32-mm-thick) encloses a homogeneous medium that represents the sediment under study. Other model parameters are given in Table 3.

[30] Initially, the soil cell system is considered at equilibrium and at temperature T_o throughout. The cell wall is maintained at constant temperature T_o throughout the model run. Heat flux is imposed at the boundary between the copper core and the wax layer at $t > 0$. Continuity is satisfied at all other internal boundaries. No boundary effects are observed during the first 300 s when either perfectly conductive or perfectly insulating cell walls are imposed.

[31] We calibrate our laboratory measurement system against the numerical model using data gathered for water that was gelled to avoid convection. This calibration allows us to determine the magnitude of the heat flux associated with a given input voltage applied to the needle probe. The calibrated numerical model is used for data reduction by performing successive forward simulations until model predictions fit experimental data. The resolution in conductivity obtained with this procedure is better than $\pm 0.1\lambda$. Figure 4 shows data and a set of numerical results generated during data reduction. The main advantage of applying a numerical simulation rather than available analytical solutions is increased confidence in data analysis. In particular, the FEM simulations give us the ability to properly capture boundary conditions, to study their impact, and to reproduce the whole time series rather than selecting a priori the range of data to be fit.

5. Results

5.1. Air Dry Sediments

[32] Thermal conductivity values for all tested sediments under air dry conditions are shown as a function of vertical effective stress in Figure 5. These data highlight the role of coordination number and contact quality, which increase with effective stress (i.e., the bottlenecks for heat conduction). The extrapolation to higher vertical effective stress levels can be taken into consideration through changes in porosity. Volume change is monitored throughout the testing history to recover the instantaneous porosity in the sediment. All specimens experience volume contraction during loading, but volume change is more pronounced in kaolinite specimens. The porosity in air dry kaolinite decreases from 0.74 to 0.61 when the vertical effective stress changes from 0.05 MPa to 1 MPa. The associated change in thermal conductivity is 0.074 W m^{-1} K^{-1} to 0.21 W m^{-1} K^{-1}. For the same vertical effective stress interval, the porosity change in air dry sand

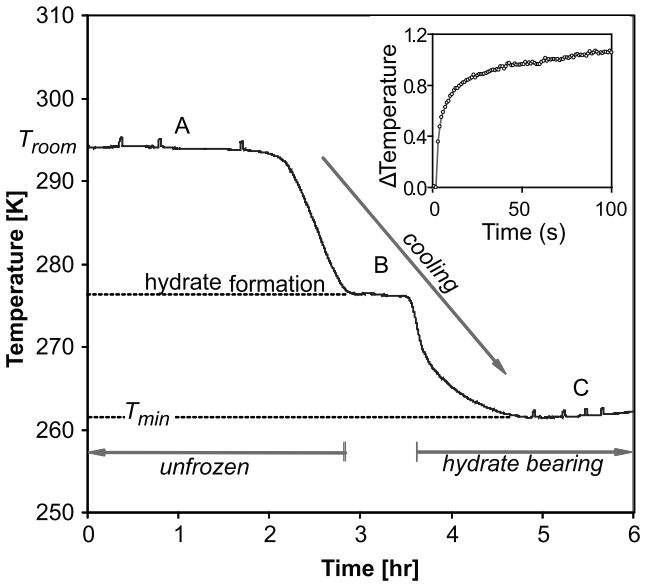

Figure 3. Typical change in temperature as a function of time for a single-load step. Temperature is monitored continuously throughout the test. Stage A is unfrozen sediment. Stage B is hydrate formation stage characterized by constant temperature. Stage C is hydrate-bearing sediment. Small peaks within stages A and C correspond to the heat pulses associated with thermal conductivity measurements. The inset shows one such measurement in detail.

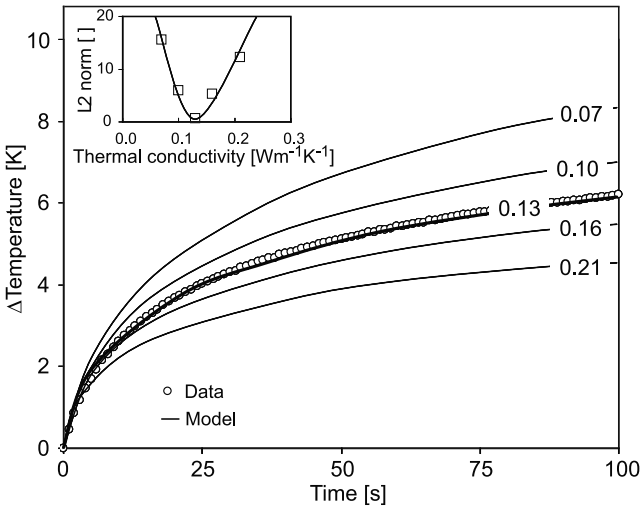

Figure 4. Temperature-time signature for a single measurement conducted on air dry kaolinite at $\sigma' = 0.25$ MPa. Numerical results obtained using COMSOL® are shown as the model curves, labeled with the corresponding thermal conductivity in units of W m^{-1} K^{-1}. The inset shows the error curve generated by the numerical model for different values of thermal conductivity.

is small (0.45 to 0.44), but the increase in thermal conductivity is pronounced (0.28 W m^{-1} K^{-1} to 0.48 W m^{-1} K^{-1}). For comparison, the rate of change of thermal conductivity relative to porosity n, as given by $\Delta\lambda/\Delta n$, is $\sim$1 W m^{-1} K^{-1} in the kaolinite and 20 W m^{-1} K^{-1} in sand.

5.2. Water Saturated Sediments (Without Hydrate)

[33] Figure 5 also shows the results for water saturated unfrozen specimens. Thermal conductivity values are much higher than for air dry conditions, highlighting the contribution of water in facilitating heat transport across contacts. The thermal conductivity of the saturated sand shows no measurable sensitivity to changes in vertical effective stress. Saturated kaolinite exhibits an increase in thermal conductivity (2.1 W m^{-1} K^{-1} to 2.8 W m^{-1} K^{-1}) for vertical effective stress increasing from 0.05 MPa to 1 MPa. The associated change in porosity is 0.67 to 0.51.

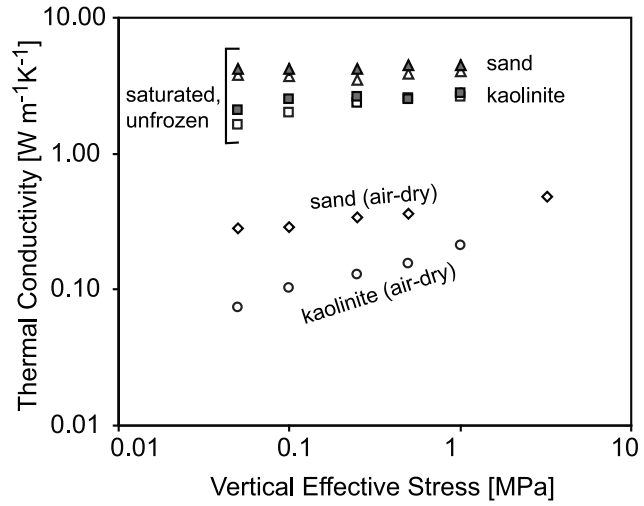

Figure 5. The thermal conductivity of dry and saturated unfrozen specimens as a function of the applied vertical effective stress under zero lateral strain. For the saturated samples, the gray symbols denote water as the wetting fluid while open symbols correspond to wetting with water + liquid THF. The uncertainties associated with each measurement are too small to be visible on this logarithmic thermal conductivity scale and are not plotted.

5.3. Specimens With THF Solution (With and Without Hydrate)

[34] The thermal conductivity data for room temperature sediments mixed with the stoichiometric THF solution as the pore-filling fluid are also shown in Figure 5. The thermal conductivity of stoichiometric THF solution at room temperature is very close to the value for water (Table 2). Therefore, the conductivity in the unfrozen state differs little between the THF- and water-saturated specimens. Differences reflect changes in porosity and fabric due to pore fluid chemistry (in the kaolin specimen) or due to densification (in the sand specimen).

[35] Figure 6 shows the thermal conductivity for THF-saturated sand and kaolinite specimens before and after hydrate formation. There is a marked increase in conductivity at low vertical effective stress in both sand (3.7 W m^{-1} K^{-1} to 4.5 W m^{-1} K^{-1}) and kaolinite (1.6 W m^{-1} K^{-1} to 2.8 W m^{-1} K^{-1}) specimens upon hydrate formation at vertical effective stress of 0.05 MPa. For these experiments, samples having 100% hydrate saturation experience volume

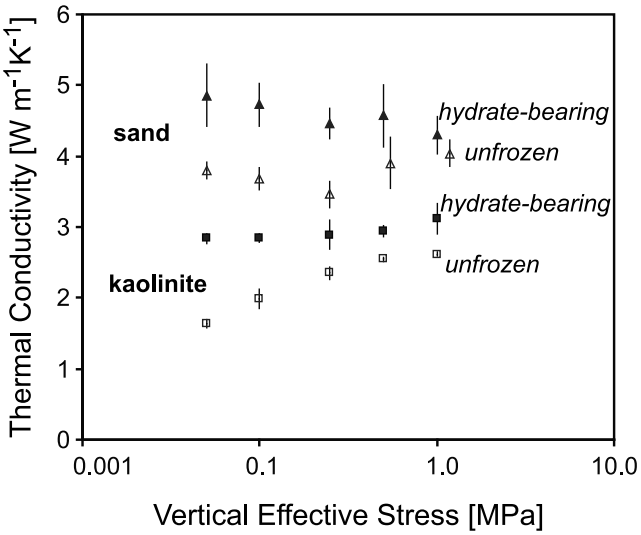

Figure 6. Thermal conductivity of hydrate-bearing sand and kaolinite (filled symbols) and saturated, unfrozen sand and kaolinite samples with water + liquid THF as the wetting fluid (open symbols) shown as a function of applied vertical effective stress. Error bars reflect the variability in thermal conductivity values obtained during multiple measurements. The best quality thermal conductivity determination is chosen as the location of the plotted symbol. To facilitate visualization, the thermal conductivities of the saturated, unfrozen sand at the two highest vertical effective stress values have been slightly shifted to higher effective stress.

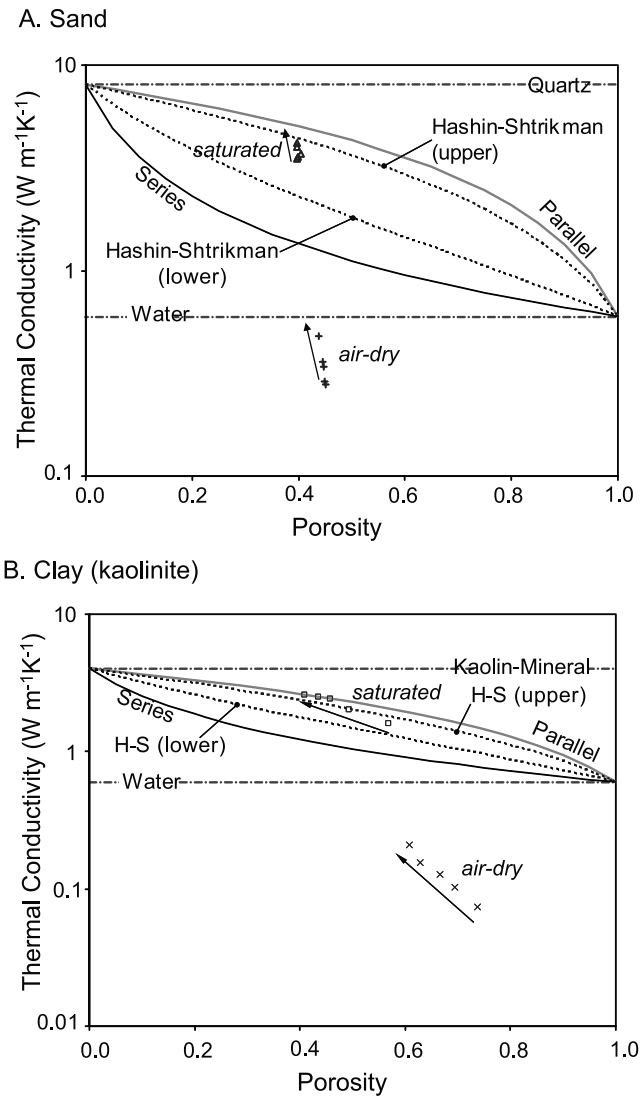

Figure 7. Thermal conductivity of dry and saturated, unfrozen (a) sand and (b) clay specimens as a function of porosity. Arrows point in the direction of increasing vertical effective stress for air dry and saturated, unfrozen samples. The plotted parallel (gray curves) and series (black curves) effective media bounds and the Hashin-Shtrikman (H-S) upper and lower bounds (dotted) are calculated for saturated, unfrozen specimens. Also shown as gray dashed-dotted lines are the end-member thermal conductivities of water and mineral grains.

expansion during hydrate formation and volume contraction upon dissociation.

6. Discussion

[36] The compiled experimental results imply that several factors affect the thermal conductivity of soils with different pore filling material and at different vertical effective stress under zero-lateral strain conditions. First, we consider the air dry specimens, whose thermal conductivities are plotted as a function of porosity in Figure 7. Two causal links between effective stress and thermal conductivity are readily identified: (1) For coarse-grained soils (sand), increased effective stress results in very little porosity reduction. Thus, the increase in thermal conductivity with effective stress σ' reflects enhanced heat transfer across contacts due to the higher interparticle contact force F, which is proportional to $d^2\sigma'$, where d is the grain diameter. (2) For fine-grained soils (kaolinite), the increase in thermal conduction is primarily caused by the large reductions in porosity, which leads to an increase in coordination number.

[37] Next we consider the saturated specimens. The liquid in the pore space contributes to thermal conduction within the fluid along the pores and creates a thermal bridge between particles, leading to particle-fluid-particle conduction (Figure 1). Replacing air with either water or the liquid THF solution increases the effective thermal conductivity of the bulk samples by a factor of ~10 (Figure 5). Clearly, the presence of liquid in pores in the samples exerts a far greater effect on thermal conductivity than does the change in effective stress. The effect of water should extend to relatively low water saturation levels as anticipated from Figure 1. Such low saturation conditions are characteristic of hydrate dissociation and gas production in natural settings.

[38] Finally, we consider the case of hydrate-bearing sediments. The thermal conductivity of THF hydrate is close to that of a liquid phase mixture of THF and water, in sharp contrast to the situation for ice and water (Table 2). It might therefore be assumed that the presence of hydrate should have little impact on bulk soil thermal conductivity. The increase that we observe in thermal conductivity in the presence of THF hydrate for both coarse- and fine-grained sediments therefore requires further analysis. We consider several hypotheses that may explain the thermal conductivity relationships noted in our data.

6.1. Experimental Bias

[39] The design or implementation of the laboratory experiments might have produced systematic problems that lead to increased thermal conductivity in the hydrate-bearing sediments. For example, if excess water were present, ice would have formed in pore space and increased the thermal conductivity of the sample. Our experiments were carefully prepared to ensure a condition of excess THF, not free water, if hydrate formation did not run to full theoretical completion (i.e., 100% occupancy of pore space). Furthermore, none of the temperature measurements (e.g., Figure 3) reveals a second phase transition plateau as would be expected in the case of a water-ice transition. Noise in the data and uncertainty in data reduction can also not account for the measured increase in thermal conductivity in the presence of hydrate; in all cases, the raw data show clear and consistent differences between specimens before and after hydrate formation.

6.2. Cryogenic Suction and Segregation

[40] The literature on ice in fine-grained soils shows that ice forms first in the larger pores. Then, the pore fluid migrates from the smaller pores toward the nucleating ice, causing cryogenic suction [*Andersland and Ladanyi*, 2004; *Hutchinson*, 1974; *Konrad*, 1989; *McRoberts*, 1975; *Miller*, 1980]. Therefore, while soils experience global volume expansion during freezing, the local porosity decreases near the freezing front.

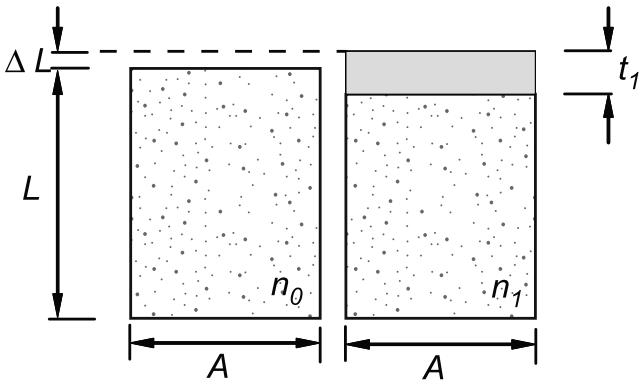

Figure 8. Fluid-saturated sediment of initial porosity n_0 and volume $A{\cdot}L$ is shown on the left. Hydrate forms at constant mass, undergoing volume expansion ($A{\cdot}\Delta L$) and occupies a segregated volume $A{\cdot}t_l$ on the right side of the diagram. The porosity n_1 of the neighboring, unfrozen saturated soil has decreased compared to initial porosity n_0 as fluid migrated to the hydrate phase.

[41] Cryogenic suction and segregation may also play an important role in controlling the thermal conductivity of hydrate-bearing sediments. The effective thermal conductivity will depend on the conductivity of the hydrate phase, the conductivity of the lower-porosity unfrozen sediment, and the relative spatial distribution of the frozen and unfrozen areas within the sample.

[42] Consider a fluid saturated sediment of initial porosity n_0 and volume $A{\cdot}L$, where A denotes area and L length (Figure 8). Hydrate forms at constant mass and occupies a segregated volume $A{\cdot}t_l$. The porosity of the neighboring, unfrozen saturated soil decreases as fluid driven by cryogenic suction migrates to the hydrate phase. Invoking mass conservation and incorporating volume expansion β of 9.89% during hydrate formation [*Sloan*, 1998], the reduced porosity n_1 for the unfrozen sediment becomes:

$$n_1 = \frac{n_0[1+\beta(1-\alpha_L)]-\alpha_L}{(1+\beta)(1-\alpha_L)}, \tag{2}$$

where α_L is the volume fraction of segregated hydrate determined from $\alpha_L = t_l/(L + \Delta L)$ with ΔL denoting the change in the specimen's length.

[43] The effective media properties of the hydrate-bearing sediment will depend on the spatial distribution of the segregated hydrate in the sample. Two of the most commonly used effective media models, parallel and series, predict different results for the case of cryogenic suction during hydrate formation. A series model, given by

$$\lambda_{series} = \left[\frac{\alpha_L}{\lambda_h} + \frac{(1-\alpha_L)}{\lambda_{\text{soil}}}\right]^{-1}, \tag{3}$$

predicts a decrease in bulk thermal conductivity λ_{series}. Subscripts h and "soil" refer to hydrate and mineral grains, respectively. The parallel model

$$\lambda_{\text{parallel}} = \alpha_L\lambda_h + (1-\alpha_L)\lambda_{\text{soil}}, \tag{4}$$

predicts increased bulk thermal conductivity $\lambda_{\text{parallel}}$, as is observed in our experiments. This would suggest that hydrate segregation in our samples occurred in the radial direction. Such hydrate segregation has also been observed in other studies [*Waite et al.*, 2008a].

[44] The increase in thermal conductivity of fine-grained soils following cryogenic suction and hydrate segregation processes should be less pronounced at high effective stress. Indeed, our experimental results show smaller changes in conduction upon hydrate formation at high effective stress in the kaolinite sample.

6.3. Increase in Effective Stress

[45] Cryogenic suction loses relevance in the case of coarse-grained soils (sand), and it therefore cannot be invoked to explain the observed increase in thermal conductivity during hydrate formation. However, volume expansion during hydrate formation produces a large increase in radial effective stress in the sample, which is maintained under zero-lateral strain conditions. Note that during volume expansion the principal stresses may even rotate, with the effective vertical stress becoming the radial stress. For coarse-grained soils, the change in thermal conductivity recorded in Figure 5 may primarily reflect the improvement in the quality of intergranular contacts during the increase in effective stress.

6.4. Reduced Interface Thermal Impedance

[46] Experimental evidence shows a temperature discontinuity across interfaces in multicomponent media [*Benveniste*, 1987; *Swartz and Pohl*, 1989]. This phenomenon cannot be attributed merely to differences in thermal conductivity between components since thermal conductivity changes produce a change in thermal gradient, not a discontinuity in temperature. For our experiments, hydrate formation in the soil samples transforms grain-liquid interfaces to grain-hydrate interfaces. The fundamental change in the nature of heat transfer from solid-liquid to solid-solid could lead to a reduction in interfacial thermal impedance and thus the observed increase in thermal conductivity. This effect should be more prevalent in clays, with the larger number of interfaces, than in sands, although our results indicate a sharper increase in thermal conductivity in sands.

7. Conclusions

[47] 1. The analytical solution for a line source in an infinite medium can be used to fit our data, but with poor resolution. We achieved lower uncertainty in thermal conductivity using a numerical model of the tested needle medium cell system.

[48] 2. Increasing the effective confining stress on granular media increases both the number of contacts (prevalent in clayey soils) and the quality of contacts (prevalent in sandy soils). A tenfold increase in vertical effective stress from an initially low stress level can cause an increase in thermal conductivity by a factor of 2 or 3.

[49] 3. Changing the pore fluid from gas (dry) to liquid (saturated) allows for additional conduction paths, namely grain-liquid-grain and through the percolating liquid phase. This results in a pronounced increase in thermal conductivity, typically by a factor of $\sim$10 or greater, between dry and

saturated samples. The presence of liquid in the pores exerts a far greater effect on bulk thermal conductivity than does a change in effective stress.

[50] 4. The thermal conductivity of sediments increases upon hydrate formation, even though hydrate and water exhibit very similar thermal conductivity values. Experimental biases fail to explain the observed changes. Several possibly coexisting physical mechanisms may be involved, including (1) cryogenic suction and hydrate segregation (fine-grained soils), (2) an increase in effective stress and improvement in contact quality as a result of increasing radial effective stress under zero lateral strain conditions (coarse-grained soils), and (3) reduction in interfacial thermal impedance as the system changes from grain-liquid to grain-hydrate. Further investigation will be necessary to assess the validity of these hypotheses and their full implications.

[51] **Acknowledgments.** This work was supported by the Chevron Joint Industry Project on Methane Hydrates under contract DE-FC26-01NT41330 to Georgia Institute of Technology from the U.S. Department of Energy's National Energy Technology Laboratory. J.C.S. received additional support from the Goizueta Foundation. C.R. thanks the Petroleum Research Fund of the American Chemical Society under AC8–31351 for early support of thermal conductivity research on hydrate-bearing sediments at Georgia Institute of Technology. Comments by W. Waite and reviewer B. Dugan improved the manuscript. Any use of a trade, product, or firm name is for descriptive purposes only and does not imply endorsement by the U.S. Government. Any opinions, findings, conclusions, or recommendations expressed herein are those of the authors and do not necessarily reflect the view of the DOE or the USGS.

References

Aduda, B. O. (1996), Effective thermal conductivity of loose particulate systems, *J. Mater. Sci.*, *31*(24), 6441–6448, doi:10.1007/BF00356246.

Andersland, O. B., and B. Ladanyi (2004), *Frozen Ground Engineering*, 384 pp., John Wiley, Hoboken, N. J.

BASF (1998), Tetrahydrofuran (THF) storage and handling, technical report, Mount Olive, N. J.

Batchelor, G. K., and R. W. O'Brien (1977), Thermal or electrical conduction through a granular material, *Proc. R. Soc. London, Ser. A*, *355*(1682), 313–333.

Becker, B. R., et al. (1992), Development of correlations for soil thermal conductivity, *Int. Commun. Heat Mass Transfer*, *19*, 59–68, doi:10.1016/0735-1933(92)90064-O.

Benveniste, Y. (1987), Effective thermal conductivity of composites with a thermal contact resistance between the constituents: Nondilute case, *J. Appl. Phys.*, *61*(8), 2840–2843, doi:10.1063/1.337877.

Buffett, B., and O. Zatsepina (2000), Formation of gas hydrate from dissolved gas in natural porous media, *Mar. Geol.*, *164*, 69–77, doi:10.1016/S0025-3227(99)00127-9.

Chung, D. D. L. (2001), Materials for thermal conduction, *Appl. Therm. Eng.*, *21*(16), 1593–1605, doi:10.1016/S1359-4311(01)00042-4.

Cook, J. G., and D. G. Leaist (1983), An exploratory study of the thermal conductivity of methane hydrate, *Geophys. Res. Lett.*, *10*, 397–399, doi:10.1029/GL010i005p00397.

deMartin, B. (2001), Laboratory measurements of the thermal conductivity and thermal diffusivity of methane hydrate at simulated in situ conditions, M.S. thesis, 155 pp., Ga. Inst. of Technol., Atlanta.

Droval, G., J. F. Feller, P. Salagnac, and P. Glouannec (2006), Thermal conductivity enhancement of electrically insulating syndiotactic poly (styrene) matrix for diphasic conductive polymer composites, *Polym. Adv. Tech.*, *17*, 732–745, doi:10.1002/pat.777.

Farouki, O. T. (1985), Thermal Design Considerations in Frozen Ground Engineering: Ground Thermal Properties, edited by T. G. Krzewinski and R. G. Tart, pp. 186–203, Am. Soc. of Civ. Eng., New York.

Gangadhara Rao, M. V. B. B., and D. N. Singh (1999), Generalized relationship to estimate thermal resistivity of soils, *Can. Geotech. J.*, *36*, 767–773, doi:10.1139/cgj-36-4-767.

Grevemeyer, I., and H. Villinger (2001), Gas hydrate stability and the assessment of heat flow through continental margins, *Geophys. J. Int.*, *145*, 647–660, doi:10.1046/j.0956-540x.2001.01404.x.

Guéguen, Y., and V. Palciauskas (1994), *Introduction to the Physics of Rocks*, 392 pp., Princeton Univ. Press, Princeton, N. J.

Guimaraes, M. (2001), Crushed stone fines and ion removal from clay slurries, Ph.D. thesis, 238 pp., Ga. Inst. of Technol., Atlanta.

Handa, Y. P. (1986), Compositions, enthalpies of dissociations, and heat capacities in the range 85 to 270 K for clathrate hydrates of methane, ethane, and propane, and enthalpy of dissociation of isobutene hydrate as determined by a heat-flow calorimeter, *J. Chem. Thermodyn.*, *18*, 915–921, doi:10.1016/0021-9614(86)90149-7.

Helgerud, M. B. (2001), Wave speeds in gas hydrate and sediments containing gas hydrate: A laboratory and modeling study, Ph.D. thesis, 271 pp., Stanford Univ., Stanford, Calif.

Henninges, J. (2007), Measurements of thermal conductivity of tetrahydrofuran-hydrate-bearing sand using the constantly heated line-source method, paper presented at International Conference 2007 and 97th Annual Meeting, Geologische Vereinigung e. V., Bremen, Germany.

Henninges, J., E. Huenges, and H. Burkhardt (2005), In situ thermal conductivity of gas-hydrate-bearing sediments of the Mallik 5L–38 well, *J. Geophys. Res.*, *110*, B11206, doi:10.1029/2005JB003734.

Huang, D., and S. Fan (2005), Measuring and modeling thermal conductivity of gas hydrate-bearing sand, *J. Geophys. Res.*, *110*, B01311, doi:10.1029/2004JB003314.

Hutchinson, J. N. (1974), Periglacial solifluxion: An approximate mechanism for clayey soils, *Geotechnique*, *24*(3), 438–443.

Jones, B. W. (1988), Thermal conductivity probe: development of method and application to a coarse granular medium, *J. Phys. E Sci. Instrum.*, *21*, 832–839, doi:10.1088/0022-3735/21/9/002.

Kaye, G. W. C., and T. H. Laby (2007), *Tables of Physical and Chemical Constants*, 16th ed., National Physical Laboratory, Middlesex, U. K. (available at http://www.kayelaby.npl.co.uk)

Klein, C. (1999), Electromagnetic properties of high specific surface minerals, Ph.D. thesis, 335 pp., Ga. Inst. of Technol., Atlanta.

Konrad, J. M. (1989), Physical processes during freeze-thaw cycles in clayey silts, *Cold Reg. Sci. Technol.*, *16*, 291–303, doi:10.1016/0165-232X(89)90029-3.

Krivchikov, A. I., B. Y. Gorodilov, O. A. Korolyuk, V. G. Manzhelii, H. Conrad, and W. Press (2005), Thermal conductivity of methane-hydrate, *J. Low Temp. Phys.*, *139*(5–6), 693–702, doi:10.1007/s10909-005-5481-z.

Lambert, M. A., and L. S. Fletcher (1997), Thermal contact conductance of spherical rough metals, *Heat Transfer, J.*, *119*(4), 684–690, doi:10.1115/1.2824172.

Lee, J. Y. (2007), Hydrate-bearing sediments: Formation and geophysical properties, Ph.D. thesis, 219 pp., Ga. Inst. of Technol., Atlanta.

Lee, J. Y., T. S. Yun, J. C. Santamarina, and C. Ruppel (2007), Observations related to tetrahydrofuran and methane hydrate for laboratory studies of hydrate-bearing sediments, *Geochem. Geophys. Geosyst.*, *8*, Q06003, doi:10.1029/2006GC001531.

Lu, S., T. Ren, Y. Gong, and R. Horton (2007), An improved model for predicting soil thermal conductivity from water content at room temperature, *Soil Sci. Soc. Am. J.*, *71*, 8–14.

McRoberts, E. C. (1975), Pore water expulsion during freezing, *Can. Geotech. J.*, *12*, 130–141, doi:10.1139/t75-012.

Miller, R. D. (1980), Freezing phenomena in soils, in *Applications in Soil Physics*, edited by D. Hillel, pp. 254–299, Academic, San Diego, Calif.

Palomino, A., and J. C. Santamarina (2005), Fabric map for kaolinite (single mineral): Effects of pH and ionic concentration on behavior, *Clays Clay Miner.*, *53*(3), 211–223, doi:10.1346/CCMN.2005.0530302.

Ross, R. G., and P. Andersson (1982), Clathrate and other solid phases in the tetrahydrofuran-water system: Thermal conductivity and heat capacity under pressure, *Can. J. Chem.*, *60*, 881–892, doi:10.1139/v82-132.

Ruppel, C. (2000), Thermal state of the gas hydrate reservoir, in *Natural Gas Hydrate in Oceanic and Permafrost Environments*, edited by M. D. Max, pp. 29–42, Springer, New York.

Santamarina, J. C., and G. C. Cho (2001), Determination of critical state parameters in sandy soils–simple procedure, *Geotech. Test. J.*, *24*(2), 185–192, doi:10.1520/GTJ11338J.

Santamarina, J. C., and C. Ruppel (2008), The impact of hydrate saturation on the mechanical, electrical, and thermal properties of hydrate-bearing sand, silts, and clay, paper presented at 6th International Conference on Gas Hydrates, Vancouver, Canada, 6–10 Jul.

Singh, D. N., and K. Devid (2000), Generalized relationships for estimating soil thermal resistivity, *Exp. Therm. Fluid Sci.*, *22*(3–4), 133–143, doi:10.1016/S0894-1777(00)00020-0.

Sloan, E. D. (1998), *Clathrate Hydrates of Natural Gases*, 705 pp., Marcel Dekker, New York.

Spangenberg, E., J. Kulenkampff, R. Naumann, and J. Erzinger (2005), Pore space hydrate formation in a glass bead sample from methane dissolved in water, *Geophys. Res. Lett.*, *32*, L24301, doi:10.1029/2005GL024107.

Sridhar, M. R., and M. M. Yovanovich (1996), Elastoplastic contact conductance model for isotropic conforming rough surfaces and comparison with experiments, *Heat Transfer, J.*, *118*(1), 3–9, doi:10.1115/1.2824065.

Stern, L. A., S. H. Kirby, and W. B. Durham (1996), Peculiarities of methane clathrate hydrate formation and solid-state deformation, including possible superheating of water ice, *Science*, *273*, 1843–1848, doi:10.1126/science.273.5283.1843.

Stern, L. A., S. H. Kirby, and W. B. Durham (1998), Polycrystalline methane hydrate: Synthesis from superheated ice, and low-temperature mechanical properties, *Energy Fuels*, *12*(2), 201–211, doi:10.1021/ef970167m.

Stoll, R. D., and G. M. Bryan (1979), Physical properties of sediments containing gas hydrates, *J. Geophys. Res.*, *84*, 1629–1634, doi:10.1029/JB084iB04p01629.

Swartz, E. T., and R. O. Pohl (1989), Thermal boundary resistance, *Rev. Mod. Phys.*, *61*(3), 605–668, doi:10.1103/RevModPhys.61.605.

Tarnawski, V. R., W. H. Leong, F. Gori, G. D. Buchan, and J. Sundberg (2002), Inter-particle contact heat transfer in soil systems at moderate temperatures, *Int. J. Energy Res.*, *26*(15), 1345–1358, doi:10.1002/er.853.

Thalmann, R. E. (1950), Thermal conductivity of dry soils, M.S. thesis, Univ. of Kansas, Lawrence.

Tréhu, A. M. (2006), Subsurface temperatures beneath southern Hydrate Ridge, *Proc. Ocean Drill. Program, Sci. Results*, *204*, 1–26, doi:10.2973/odp.proc.sr.204.114.2006.

Tzirita, A. (1992), In situ detection of natural gas hydrates using electrical and thermal properties, Ph.D. thesis, 220 pp., Texas A&M Univ., College Station.

Vargas, W. L., and J. J. McCarthy (2001), Heat conduction in granular materials, *AIChE J.*, *47*, 1052–1059, doi:10.1002/aic.690470511.

Von Herzen, R., and A. E. Maxwell (1959), The measurement of thermal conductivity of deep-sea sediments using the needle-probe method, *J. Geophys. Res.*, *64*, 1557–1563, doi:10.1029/JZ064i010p01557.

Waite, W. F., B. J. deMartin, S. H. Kirby, J. Pinkston, and C. D. Ruppel (2002), Thermal conductivity measurement in porous mixtures of methane hydrate and quartz sand, *Geophys. Res. Lett.*, *29*(24), 2229, doi:10.1029/2002GL015988.

Waite, W. F., W. J. Winters, and D. H. Mason (2004), Methane hydrate formation in partially water-saturated Ottawa sand, *Am. Mineral.*, *89*(8), 1202–1207.

Waite, W. F., L. Y. Gilbert, W. J. Winters, and D. H. Mason (2005), Thermal property measurements in Tetrahydrofuran (THF) hydrate and hydrate-bearing sediment between −25 and +4°C, and their application to methane hydrate, paper presented at 5th International Conference on Gas Hydrates, Tapir Acad., Trondheim, Norway.

Waite, W. F., T. J. Kneafsey, W. J. Winters, and D. H. Mason (2008a), Physical property changes in hydrate-bearing sediment due to depressurization and subsequent repressurization, *J. Geophys. Res.*, *113*, B07102, doi:10.1029/2007JB005351.

Waite, W. F., J. P. Osegovic, W. J. Winters, M. D. Max, and D. H. Mason (2008b), Seeding hydrate formation in water-saturated sand with dissolved-phase methane obtained from hydrate dissolution: A progress report, paper presented at 6th International Conference on Gas Hydrates, Vancouver, Canada, 6–10 Jul.

Yagi, S., and D. Kunii (1957), Studies on effective thermal conductivities in packed beds, *AIChE J.*, *3*, 373–381, doi:10.1002/aic.690030317.

Yamano, M., S. Uyeda, Y. Aoki, and T. H. Shipley (1982), Estimates of heat flow derived from gas hydrates, *Geology*, *10*, 339–343, doi:10.1130/0091-7613(1982)10<339:EOHFDF>2.0.CO;2.

Yun, T. S., and J. C. Santamarina (2007), Fundamental study of thermal conduction in dry soils, *Granul. Matter*, *10*, 197–207, doi:10.1007/s10035-007-0051-5.

Yun, T. S., J. C. Santamarina, and C. Ruppel (2007), Mechanical properties of sand, silt, and clay containing synthetic hydrate, *J. Geophys. Res.*, *112*, B04106, doi:10.1029/2006JB004484.

D. Cortes and J. C. Santamarina, School of Civil and Environmental Engineering, Georgia Institute of Technology, Atlanta, GA 30332-0355, USA. (douglas.cortes@ce.gatech.edu; carlos@ce.gatech.edu)

F. M. Francisca, Facultad de Ingenieria, Universidad Nacional de Cordoba, Cordoba 5000, Argentina. (ffrancis@gtwing.efn.uncor.edu)

A. I. Martin, Atlanta, GA 30332, USA. (ana_isabel_martin@yahoo.com)

C. Ruppel, U.S. Geological Survey, 384 Woods Hole Road, Woods Hole, MA 02543, USA. (cruppel@usgs.gov)

T. S. Yun, Department of Civil and Environmental Engineering, Yonsei University, Shinchon Dong 134, Seoul, 120-749, South Korea. (taesup.yun@gmail.com)